Cortical Constraints in fully automated Non-Linear Spatial Normalization of 3D Brain Images

D.L. Collins[†], G. Le Goualher[†], C. Barillot[‡], A.C. Evans[†]

[†]McConnell Brain Imaging Center, Montreal Neurological Institute, McGill University, Montreal, Canada
[‡]Laboratoire SIM, Faculté de Médecine, Université de Rennes I, 35043 RENNES Cedex France

Abstract

Numerous techniques now exist for automatic voxel-based non-linear registration of human brains based on blurred intensity or gradient magnitude images. However, these techniques generally fail to achieve a high degree of alignment for corresponding cortical sulci from different brains. In earlier work [1] on simulated data, we demonstrated that cortical registration could be improved by using blurred, geometric, image-based features (L_{vv}) or explicitly labelled sulcal traces. In order to improve registration in real MRI data, the technique is now modified to incorporate explicitly labelled sulcal ribbons in conjunction with a chamfer distance objective function. Experiments with 10 simulated data sets demonstrate a 56% reduction in residual sulcal registration error (from 3.4 to 1.5mm, on average) when compared to automatic linear registration and a 28% improvement over our previously published non-linear technique (from 2.1 to 1.5mm). The simulation results are confirmed by experiments with real MRI data from young normal subjects, where sulcal misregistration is reduced by 20% (from 5.0mm to 4.0mm) and 11% (from 4.5 to 4.0mm) over the standard linear and nonlinear registration methods, respectively.

I. Introduction

The interpretation of functional brain images in brain mapping is usually aided by comparison to an atlas or to similar data from other subjects [2]. Unless a matched anatomical (MR or CT) image is available for each subject, anatomical variability must be taken into account to avoid over interpretation of the individual's functional data [3]. The origins and ramifications of variation in functional neuroanatomy in the normal population are poorly understood. Furthermore, estimation of spatial variability depends intimately on the selected frame of reference. More often than not, anatomical landmarks are used to determine the frame of reference. Any spatial variability of functional regions will be a composite of each subject's anatomy and the positional variability of functional regions on the anatomical substrate. Quantification and interpretation of functional variability is possible only after anatomical variability has been accounted for. These issues are central to the International Consortium for Brain Mapping (ICBM) project, where the main aim is to develop neuroinformatics tools to build a probabilistic reference system of the human brain [4]. As one of the ICBM members, we have therefore been interested in automatic procedures to capture and quantify anatomical differences between normal brains based on their appearance in 3D MRI. We have concentrated mainly on fully automatic procedures since manual intervention is time consuming, especially when applied to ensembles of volumetric image data from large numbers ($n > 100$) of subjects. Furthermore, inter and intra-observer variability in structure labelling or landmark identification may reduce detectability of small differences

between groups. Towards the goal of automated analysis of anatomy, we have developed a program called ANIMAL (Automatic Nonlinear Image Matching and Anatomical Labelling) [5].

The ANIMAL procedure is based on the assumption that different brains are topologically equivalent and that non-linear deformations can be estimated and applied to one data set in order to bring the anatomy of one into correspondence with another. This registration process is then used (i) to estimate non-linear morphometric variability in a given population [6], (ii) to automatically segment MRI data [5], or (iii) to remove residual alignment errors when spatially averaging results among individuals.

Our previous validation of ANIMAL showed that it worked well for deep brain structures and ventricles [5], but often had difficulty aligning sulci and gyri. In a subsequent paper [1], we described an extension of the basic non-linear registration method that used additional image-based features to help align the cortical mantle. Simulations showed that L_{vv}-based features and blurred sulcal traces significantly improved cortical registration. However, these results were not confirmed with real data in our previous work largely because of the difficulty in automatically establishing correspondence between sulci in different brains. In this paper, we demonstrate that the use of automatically extracted and labelled sulci as extra features in conjunction with a chamfer distance objective function [7], [8] shows significant improvement over our previous work for both simulated and real MRI data.

In contrast to existing methods for cortical structure alignment that depend on manual intervention to identify corresponding points [9], [10] or curves [11], [12], [13], [14], or a combination of features [15], [16], the procedure presented here is completely automatic. While many 3D voxel-based non-linear registration procedures exist (e.g., [17], [18], [19], [20], [21]), most have not specifically examined the question of cortical features for cortical registration. The work presented in [15], [16] is an exception, where point, curve and volumetric intensity data are used to drive the registration. Like the surface-matching algorithms described in [13], [22], [23] or to the multiple feature-based work described in [15], [16], the method presented here explicitly uses sulcal information to improve cortical registration. In contrast to these latter methods, our method requires no manual intervention for landmark or feature identification.

The paper is organized as follows: Section II describes previous work on non-linear registration methods applied to the human brain; Section III describes the creation of simulated data using a digital brain-phantom, the acquisition parameters for real MRI data and the non-linear

registration method; The first part of Section IV presents experiments on simulated MRI data with known deformations in order to compare our standard linear and non-linear registration procedures with the new technique and to determine a lower-bound for the registration error; the second half of Section IV describes experiments on 10 real MRI data sets, comparing the old and new registration methods. The paper concludes with a discussion and presents directions for further research.

II. Previous work

Nonlinear warping of brain images for image registration and atlasing is not new. A number of different features can be used as input data to drive the non-linear registration process. These include volumetric image data, extracted surfaces to represent the cortex or lines (and surfaces) to represent sulci. In 1981, Broit *et al.* [24] were among the first authors to describe an automatic procedure to deform an atlas image onto a CT image of the brain. They modeled the atlas as a continuous elastic solid and simulated the physical deformations required to bring the cortical and ventricular boundaries from the atlas into correspondence with those of subject's CT data. This work was continued by Bajcsy [25], and extended to 3-D [26], [17]. Gee *et al.* [19], [27] have extended the technique further by including a probabilistic approach to account for uncertainties involved in the matching process, where the Bayesian estimate of the transformation represents an optimal interpretation of an *a posterior* model.

The group at Washington University also use a probabilistic formulation with physically-based models to constrain the registration problem [28]. Christensen extended this method to 3-D and included a Karhunen-Loeve model for linear elastic deformations [18]. The quadratic-based regularization models used by all groups cited this far are all limited by the so-called *small deformation* assumption in order to maintain topology. The small deformation constraint ensures that the determinant of the jacobian remains non-negative throughout the deformation field, and thus the continuum requirement (no tearing, no folding) is maintained. Large scale deformations are easily effected through multi-scale implementations (e.g., [17], [18]), where the solution at each scale statisfies the small deformation requirement.

However, in order to achieve large local non-linear displacements while maintaining continuity in the deformation, Christensen *et al.* replaced the linear elastic constraints with a viscous fluid model [29], [15]. The implementation uses a dual hierarchy on both data and fitting strategy to deal with the increased difficulty incurred by the immense search space. A hierarchical fitting

strategy is combined with multi-scale data that (1) estimates an affine transformation, (2) uses a linear elastic basis model to estimate an initial non-linear transformation [28], [18], and (3) finishes with a fluid transformation to correct any residual differences [29]. This group has extended their work in non-linear fluid-based transformations to explicitly use cortical features by combining constraints from points, lines, surfaces and/or volumes as a solution of a generalized Dirichlet problem to improve the mapping from one brain to another [15], [16]. By using manually identified lines to represent sulci, they were able to successfully register cryosection data from one macaque monkey brain to another, and by using manually identified landmarks on the head and hippocampus of a human subject from T1-weighted MRI data they were able to register and segment the hippocampus from another subject.

A number of parametric deformation procedures also exist and are described quickly here. In the methods developed by Friston *et al.* [30], [31], the deformation is constrained to consist of a linear combination of smooth basis warps that are defined by discrete cosine transforms. When training data is available, modal analysis [32] allows one to change from predefined basis functions to the eigenmodes of the training set's deformation matrix. Cootes *et al.* [33] take advantage of a similar methodology, describing objects with a set of boundary points and then using principal component analysis to determine the object's modes of variation (eigenvectors corresponding to the largest magnitude eigenvalues) among corresponding points on different objects. Székely [34] extended the concept by using automatic shape parameterization for any surface with a sphere topology, removing a dependence on one-to-one point correspondence in the different training sets required by Cootes. In each of these parametric methods, weighting factors (i.e., eigenvalues) are found that maximize a similarity criterion between source and target volumes (or objects). While the least-squares solution can be found quickly, the deformations recovered are limited by the predefined basis warps, or by the variation present in the training set.

With the exception of [15], [16], the methods described above do not explicitly use cortical features to improve registration at the cortex. Ge *et al.* [35], [11] have used manually identified sulci in conjunction with a thin-plate spline interpolant to register brain scans from multiple subjects. In our lab, Luo *et al.* [12] have used manually-traced non-labelled sulci and an iterative closest point (ICP) algorithm to register sulci with a polynomial deformation. A similar registration algorithm was developed by Subsol *et al.* [36], using automatically extracted crest-lines instead of sulcal traces. Crest-lines extracted from the ventricular surface that were common to multiple

data sets were used to build a ventricular atlas [37], however the method has not yet been used satisfactorially to produce a cortical atlas, possibly since ICP does not deal well with the greater anatomical variability at the cortex. In each of these sulcal-based methods, the deformation required to align sulci may be applied to the rest of the MRI data set for volumetric registration.

While the aforementioned methods align sulcal traces[1] quite well, they do not necessarily register the cortical mantle. Extra information, such as the cortical surface, must be used to ensure that the cortex between sulci (i.e., gyri) is also aligned. Sandor [13], Thompson [22] and Davatzikos [23] each have presented methods that begin by automatically extracting the cortical surface followed by manual identification of a small number of sulci that are used to constrain the registration. Sandor [13] modeled the surface with cubic b-splines and used conjugate gradient optimization to minimize the sum of an elastic energy potential and two chamfer distance functions; one estimating sulcus-to-sulcus distance and the other measuring cortical surface-to-surface distance. The topology of the cortical surfaces used by Thompson and Davatzikos is equivalent to a sphere, permitting them to simplify sulcal matching by computing on the 2D surface instead of 3D space. Thompson [22] estimated the polar-coordinate remapping required to match corresponding sulci by optimizing a displacement field that is represented by a weighted sum of spherical harmonics. Davatzikos [23] applied multi-resolution over-relaxation to maximize sulcal overlap while minimizing a elastic energy potential on the 2D surface. While these methods yield good results near the surfaces used in the procedures, the registration quality for deep brain tissue depends entirely on the interpolant used to map the "cortical-surface warp" into a "volumetric warp". Both authors address this problem by including some additional surfaces to represent deep structures, fissures and other sulci. In contrast, the method presented here computes the volumetric warp directly using all of the image intensity information within the volume.

In addition, our method explicitly uses sulcal information like Sandor [13], Thompson [22], Davatzikos [23] or Christensen [15] to improve cortical registration. It is important to note that the main difficulty addressed here is that of *correspondence* since automatically extracted and labelled sulci are used to drive the registration procedure, while correspondence is established manually in the aforementionned procedures. Any errors in sulcal identification will lead to misregistration errors. Still, experimental results presented below indicate that such data can

[1] A sulcal trace is the 1D curve representing an idealized sulcus on the external surface of the cortex.

improve inter-subject registration of cerebral data from human subjects.

The volumetric non-linear registration procedure (ANIMAL) is similar to that developed by Bajcsy [17], Gee [19] or Christensen [18] except that we do not explicitly use elastic constraints in the optimization process. Instead, the deformation is estimated in a two step procedure: matching followed by regularization by smoothing the deformation field. Finally, the procedure is posed in a hierarchical multi-scale fashion so that blurred data is used at the beginning when estimating large deformations, and less blurred data is used in subsequent iterations that refine the registration.

III. METHODS.

This section begins by describing the type of data used in the matching process. A summary of the non-linear registration method is then presented with emphasis on the enhancements to explicitly include cortical features in the objective function. The section ends with a description of the these image-based cortical features.

A. Input Data

Two series of experiments are presented below (results in section IV): the first involves simulations to validate the algorithm and the second analyzes real MRI data from normal subjects to evaluate the algorithm's behavior under realistic conditions. Simulations are required to validate any image processing procedure since it is difficult, if not impossible to establish ground truth with in-vivo data. Simulations establish necessary but not sufficient conditions for the validation of the registration method for the case where complete sulcal correspondence exists among all brains. Real data are used to assess performance when this is not the case.

A.1 Simulated data

Here, we simulate MRI volumes [38] from different anatomies by warping a high resolution brain phantom [39] with a random (but known) deformation. Since both the deformation and structural labels for every voxel and cortical feature are known *a priori* , we can directly compute objective measures of the algorithm's registration performance.

A.1.a Simulated MRIs. Magnetic resonance images are simulated by MRISIM [38], a program that predicts image contrast by computing NMR signal intensities from a discrete-event simulation of pulse sequences based on the Bloch equations. In order to simulate realistic MRI

images of the human brain using MRISIM, a realistic high-resolution brain phantom [39] was used to map tissue intensities into MR images. The simulator accounts for the effects of various image acquisition parameters by incorporating partial volume averaging, noise and intensity non-uniformity (see Fig. 1). The images were simulated using the same MR parameters as those described below (section III-A.2) for the real MRI acquisitions.

A.1.b Simulated deformations. Previous work in our laboratory used ANOVA to separate inter and intra-observer variability from inter-subject anatomical variability from a collection of 30 point landmarks identified by 5 anatomists on 17 brains in stereotaxic space [40]. This work estimated anatomical variability to be on the order of 4 to 7mm in 3D for deep brain and cortical structures, respectively. This data was used to generate random spatial deformations that were applied to the brain phantom to build a family of homologous, but morphologically different brain phantoms. An MRI volume was simulated for each member of the family. The random spatial deformations were generated by defining a set of twenty point landmarks within the target brain volume[2]. A second deformed set of landmarks was produced by adding a random displacement to each of the original landmark coordinates.

A Gaussian random number generator with a standard deviation of $5mm$ was used to produce the individual components of the displacement vector. The two resulting point sets (original and deformed) were then used to define a continuous 3-D thin-plate spline (TPS) transformation function [41]. Ten such deformations were generated and used to resample the tissue volumes defining the brain phantom used to create the original target data, thus producing 10 spatially warped source data sets for testing. The average deformation magnitude was $7.7mm$ with a maximum of $19.7mm$ (Note that the TPS transformation can create deformations larger than the displacements used to define the transformation through a lever effect of nearby control points.) Figure 1 shows transverse slices (after linear stereotaxic registration) through the original and three of the ten warped volumes used in the experiments below. While these images demonstrate

[2]The points were distributed in the following manner: On the midline: anterior commissure (AC), superior aspect of the splenium of the corpus callosum, center of the fourth ventricle, ventral aspect of the pons, intersection of transverse and straight sinus, parieto-occipital notch (projected to the midline), most superior aspect of brain at midline, frontal pole (projected to the midline). Bilaterally: anterior aspect of the temporal poles, center of Heschl's gyrus, of the inferior frontal gyrus, of the inferior temporal gyrus, of the supplementary motor area, the fundus of central sulcus at intersection of coronal plane passing through the posterior commissure. (Note that these are not the same points used in [40])

extreme deformations, they form a good test for ANIMAL .

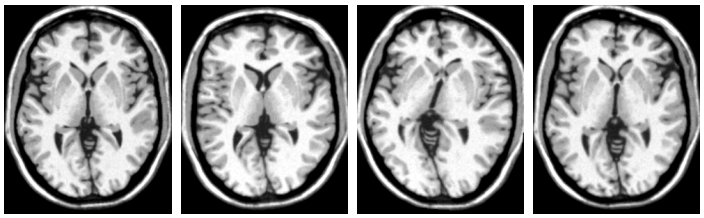

Fig. 1. Data for simulations: This figure shows transverse slices (z=10mm, in stereotaxic space) for four of the ten simulated test volumes, generated by deforming a template volume. These volumes are perhaps deformed more than one would typically find in the normal population. However, subjects representing an extreme of normal anatomical variability could exhibit such distortions. Note that while only 2-D images are shown in the figures, all calculations are computed in 3-D on volumetric data.

A.2 MRI Acquisition

In the second series of experiments, real MRI was used to validate ANIMAL . Ten subjects were selected from a data base of 150 young normal subjects that were acquired as part of the ICBM project [4]. These data were scanned on a Philips Gyroscan ACS 1.5 Tesla superconducting magnet system at the Montreal Neurological Institute using a T1-weighted 3-D spoiled gradient-echo acquisition with sagittal volume excitation (TR=18, TE=10, flip angle=30^o, 1mm isotropic voxels, 140-180 sagittal slices). These data sets were non-linearly registered to the same target used for the simulation experiments.

B. Processing Pipeline

A number of processing steps are required to register two data sets together. We have combined preprocessing steps (image intensity non-uniformity correction [42]), linear registration (ANIMAL in linear mode [43]) and resampling into stereotaxic space, cortical surface extraction (MSD [44], [45]), tissue classification (INSECT [46]), automatic sulcal extraction (SEAL [47]) and non-linear registration (ANIMAL in nonlinear mode [5]) into a processing pipeline. These are represented schematically in Fig. 2. Central to this processing is the concept of *stereotaxic space*, a brain-based coordinate system that permits direct voxel-by-voxel comparison of multiple data sets brought into this space, permits the use of spatial masks and anatomical priors, provides a means for voxel-based statistical analysis and facilitates longitudinal and between-group analysis

[48]. After running this basic pipeline, a subject's MRI volume can be visualized in stereotaxic space with its corresponding tissue labels, anatomical structure labels, cortical surface and sulcal ribbons — all in 3D. Since they are at the heart of the work presented here, the registration and sulcal extraction procedures are described in more detail below.

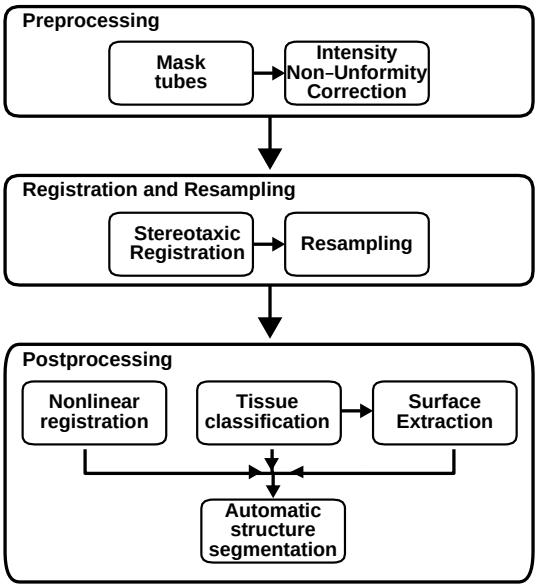

Fig. 2. Processing pipeline: All MRI data (real and simulated) is processed through the pipeline shown above. After preprocessing and stereotaxic registration, the cortical surface is extracted and the MRI data is classified into grey-matter, white-matter and cerebrospinal (CSF) components. The latter is used by SEAL to extract all sulcal ribbons from the cerebral hemispheres.

B.1 Registration Algorithm

Spatial registration is completed automatically as a two step process. The first [43] accounts for the linear part of the transformation by using correlation between Gaussian-blurred features (described below) extracted from both volumes. After automatic linear registration, there remains a residual non-linear component of spatial mis-registration among brains that is largely due to normal positional variability of homologous anatomical structures. In the second step, ANIMAL estimates the 3D deformation field [5], [6] required to account for this variability.

We assume that the deformation field is a continous spatial mapping that varies smoothly over the entire field and that it can be described as "locally translational", i.e., within a small neighbourhood, the deformation field can be approximated by a translational flow field. The deformation field is built in a piece-wise linear fashion, fitting cubical neighbourhoods in sequence.

Cubes are arranged in a 3D lattice to fill the volume and each cube moves within a range defined by the lattice-spacing in order to improve similarity between the source and target volumes. At each lattice-node n_i, the deformation vector required to achieve local registration between the target cube and the corresponding cube in the subject's volume is found by optimization of 3 translational parameters (tx_i, ty_i, tz_i) that maximize the normalized correlation statistic, evaluated only in the local neighbourhood of n_i. The algorithm is applied iteratively in a multi-scale hierarchy, so that image blurring and lattice size are reduced after each iteration, thus refining the fit. At the end of the procedure, ANIMAL yields a deformation field that can be as dense as one deformation vector per voxel. Since the algorithm has been previously described in detail [5], [49], we will concentrate here only on the enhancements required to include explicitly defined cortical features in the following sections.

B.2 Features

The objective function maximized in the optimization procedure measures the similarity at every voxel between feature maps extracted from the source and target volumes. The features used in registration are shown in Fig. 3 and described below.

B.2.a Gaussian Blurring and Gradient Magnitude. We use blurred image intensity and blurred image gradient magnitude, calculated by convolution of the original data with zeroth and first order 3D isotropic Gaussian derivatives in order to maintain linearity, shift-invariance and rotational-invariance in the detection of features. Since both linear and non-linear registration procedures are computed in a multi-scale fashion, the original MR data was blurred at two different scales[3]: FWHM =8, and $4mm$, with the FWHM = (2.35σ) of the Gaussian blurring kernel acting as a measure of spatial scale. These features were found to be sufficient to achieve registration of basal ganglia structures [5]. Unfortunately, the gradient magnitude feature did not sufficiently constrain the tangential component of the deformation at the cortex. Other features had to be found here to address this weakness.

B.2.b Explicitly Extracted Sulci. The enhanced version of ANIMAL described here uses geometric features such as sulci to improve cortical alignment. We have previously reported an automated method called SEAL (Sulcal Extraction and Automatic Labeling) to extract cortical sulci (defined by the 2D surface extending from the external sulcal trace at the cortical surface

[3]FWHM = full width at half maximum

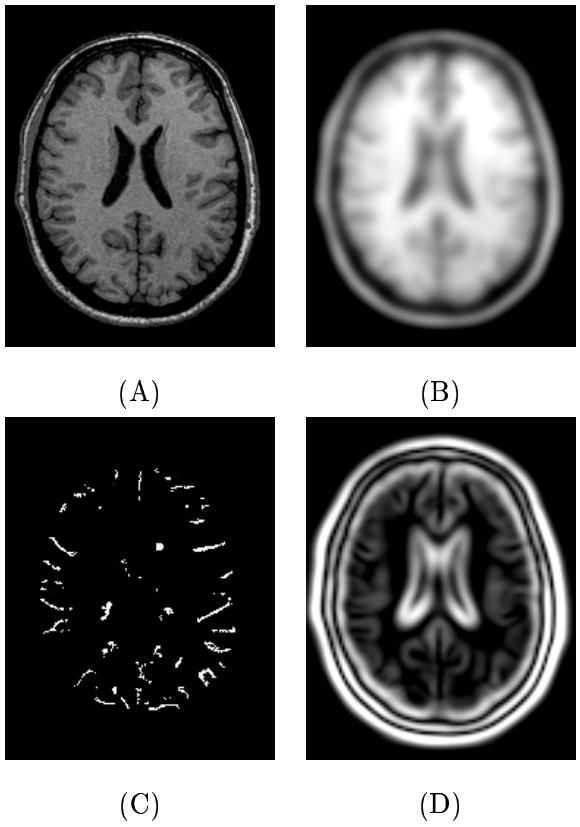

Fig. 3. Features used in registration: This figure shows a transverse slice (z=25mm in stereotaxic space) through the feature volumes used in the experiments. A) The original data; B) the blurred image intensity (FWHM = 8mm); the Elementary Sulcal Surface (ESS) voxels; and D) the gradient magnitude. The gradient magnitude and ESS voxels are complementary in the cortical region in the sense that the edges extracted by gradient magnitude are parallel to the cortex while the ESS voxels constrain the registration tangent to the cortex (see section III-B.2.b).

to the depth of the sulcal fundus) from 3D MRI [50], [47]. The sulcal ribbons (without labels) are extracted in a two step process using an active model similar to a 2D Snake that we call an *active ribbon*. First, the superficial cortical trace of the sulcus is modeled by a 1D snake-spline [51] that is initialized to loci of negative curvature of the cortical surface. This snake is then submitted to a set of forces derived from (1) tissue classification results, (2) differential characteristics of the image intensities near the cortex and (3) a distance-from-cortex term to force the snake to converge to the sulcal fundus[4]. The set of successive iterative positions of the 1D snake define the sulcal medial axis. These loci are then used to drive a 2D active ribbon which

[4]Imagine *flossing* a sulcus.

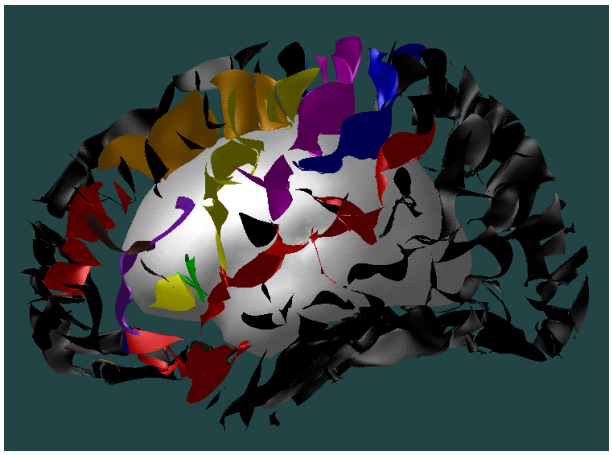

Fig. 4. Sulci extracted by SEAL : The sulci are automatically extracted and labelled by SEAL . Some manual intervention may be necessary to correct mis-labellings, however no manual corrections were applied for the data used in the experiments described below. A featureless cortical surface is shown at 50% scale to assist in orientation.

forms the final representation of the sulcus. When applied to an MRI brain volume, the output of this automatic process consists of a set of *Elementary Sulcal Surfaces* (ESS) that represent all cortical sulcal folds. Typically, 250 ESSs are extracted per hemisphere representing primary, secondary and tertiary sulci. A number of these ESSs may be needed to represent a single sulcus as defined by an anatomist since some sulci may be represented by two or more distinct sulcal folds. Validation in [52] has shown that on average, the automatically extracted surfaces are between .9 and 1.4mm away from the set of corresponding manually labeled sulcal voxels.

As shown in the experiments below, simply using unlabelled sulcal ribbons as features to be matched is not sufficient to improve cortical registration because of the difficulty in establishing correspondence between sulci in different brains. The sulci must be labelled in order to avoid sulcal (and gyral) mis-matches in the registration process. In the experiments below, sulci were identified automatically using a stereotaxic probabilistic atlas of sulcal anatomy derived from a set of 51 manually labelled graphs [53], [54]. Probabilistic identification of each ESS is achieved by integrating each sulcal spatial distribution map over the ESS surface. The ESS is assigned the label of the sulcal map with the highest probability. Methodological details can be found in [47], [53], [54].

For validation, a neuroanatomical expert[5] manually identified all ESSs in the frontal lobe [55]

[5]A medical student with neuro-anatomical expertise, under the supervision of a staff neuroanatomist specializing

using software that permits visualization of 3D surfaces as well as tri-plane (coronal, sagittal and transverse) roaming through the volume with arbitrary pan and zoom [56]. These data are used to quantitatively evaluate the nonlinear registration procedure.

B.3 Similarity Function and Fitting Strategy

The objective function used by ANIMAL to evaluate the match between source and target volumes has a classical formulation of a summation of similarity and cost terms evaluated at each node of a 3D lattice in order to align similar nearby regions. The standard procedure [5] used correlation between blurred intensity images or blurred gradient magnitude images. The multiresolution strategy used by ANIMAL had the benefit of avoiding local minima due to region mis-match and faster execution. Large blurred neighbourhoods are used at first to determine large deformations and smaller neighbourhoods (with less blurring) were used as to refine the fit as the algorithm progresses. While the standard procedure works well in general, there are two main reasons to change the objective function and the fitting strategy used by ANIMAL .

First, it is important to note that there exists important variability among subjects both for shape and spatial position[6] of cortical sulci. Unfortunately, sulcal variability is large enough to cause mismatches between unlabelled sulci since regional homology (and thus correspondence) is defined by proximity and neighbourhood similarity within ANIMAL . For example, the procedure can easily match the region of the pre-central sulcus of one subject with the central sulcus of the target, since normal anatomical variability may cause these two sulci to be better aligned after linear stereotaxic registration than the true homologous sulci. Even though these two regions may be incorrectly matched anatomically, ANIMAL will maintain their (mis-)registration if the features of their local neighbourhoods are sufficiently similar. In order to avoid such errors, labelled features (i.e., sulci) must be used in addition to proximity to establish correspondence between cortical regions.

Second, there are cases where non-corresponding sulci were incorrectly matched because they simply were not visible in the initial blurred data volumes when large deformations are estimated. When these sulci became apparent at finer scales in the multiresolution process, the reduced size of the local neighbourhood and the reduced search space did not allow deformations large enough to correct the mismatch established at the previous scale step.

in frontal lobe anatomy.

[6]Topological variability of sulcal pattern will be addressed in the discussion.

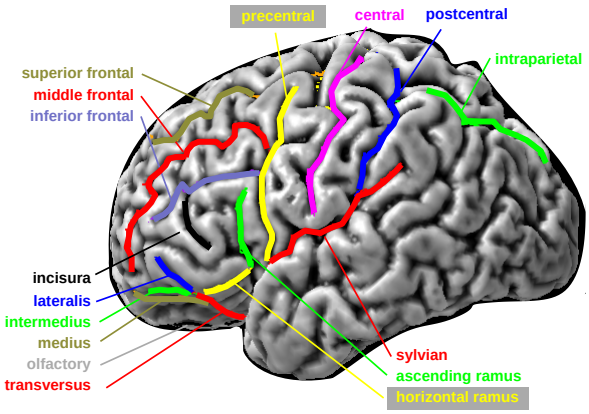

Fig. 5. Sulci used in experiments: This figure shows the 16 sulci used to evaluate the non-linear warps, overlaid on the cortical surface automatically extracted by MSD from an MRI volume. The central, Sylvian, olfactory, superior frontal and middle frontal sulci were used to drive the initial stages of non-linear fitting.

In order to avoid these two situations, the sulci must be available at the very beginning of the fitting process. Simply blurring voxel representations of the sulci so that they could be directly incorporated into ANIMAL for correlative matching did not improve cortical registration for real MRI data even though simulation results were very promising [1]. In this paper, we use a different objective function to incorporate the geometric ESS information. The sulcal ribbons are voxelated onto a 1mm^3 grid, registered with the original MRI data and a chamfer distance function [7], [8] is used to evaluate position similarity between sulci of the source and target volumes. This new method has the advantage of using an explicit representation of labelled sulci, thus alleviating the two problems described above since it can bring sulci that are initially far apart into registration.

In order to preserve the hierarchical operation of the ANIMAL process, the following fitting strategy is used: For the first low-resolution fits, only a few major sulci are included to drive the main cortical regions into registration. In the experiments described below, five pairs of sulci were identified from the ESS sets on all brain volumes corresponding to the central (Rolando), lateral (Sylvian), superior frontal, inferior frontal and olfactory sulci on both the left and right hemispheres (see Fig. 5). The use of these labelled features removes possible ambiguity in matching, since sulcal correspondence is defined before non-linear matching is initiated. For the last high resolution fits, all sulci extracted by SEAL are included to refine the non-linear deformation.

C. Error measures

The distance between manually labelled corresponding sulci was used to quantify mis-registration at the cortex and to compare the different registration strategies presented in the experiments below. This distance was estimated by D_{surf}, a 3D root mean square (rms) minimum distance measure, computed between the automatically extracted and manually *labelled* sulcal ribbons. The D_{surf} measure was defined on a point-wise basis, computing the square root of the mean square (over all control points[7] defining the set of ESS quadmeshes used to represent a given sulcus) of the minimum distance between each point in the transformed source sulcus and its nearest homologue in the target sulcus surface:

$$D_{\mathsf{surf}} = \frac{1}{2}\left(\sqrt{\frac{1}{n}\sum_{i=0}^{n-1}(d_{\mathsf{min}}(p_i))^2} + \sqrt{\frac{1}{m}\sum_{j=0}^{m-1}(d_{\mathsf{min}}(q_j))^2}\right). \quad (1)$$

Where there are n control points p_i on the transformed sulcus, m control points on the target sulcus, and $d_{\mathsf{min}}(x)$ is the Euclidean distance between the control point x and the closest point on the quadmesh representing the matching sulcus.

Since the beginning and end of many sulci were difficult to identify manually, we did not want to overly-penalize the registrations when one manually sulcus was longer (or shorter) than its homologue in the target volume. Therefore, any pair of corresponding points that includes an *edge*-point is ignored when computing the mean and the values of m and n are modified accordingly. Thus, D_{surf} indicates misregistration between the overlapping parts of the sulci only (see Fig. 6). Note that in general for real data, explicit point correspondence on the sulcal ribbons does not exist. We assume that the closest point after non-linear registration *is* the correct homologue.

For the experiments below, the 16 sulci shown in Fig 5 were labelled manually by a neuroanatomically-trained expert on the simulated phantom volume and on the real MRI volumes. The D_{surf} measure minimizes intra-observer variability error (compared to, manually labelling sulcal voxels, for example), since the sulci are automatically extracted (and thus their spatial positions are robustly defined) and only manually *labelled*.

[7]Spacing between quadmesh control points is typically less than 1mm, and a single ESS is represented by approximately 15×40 points.

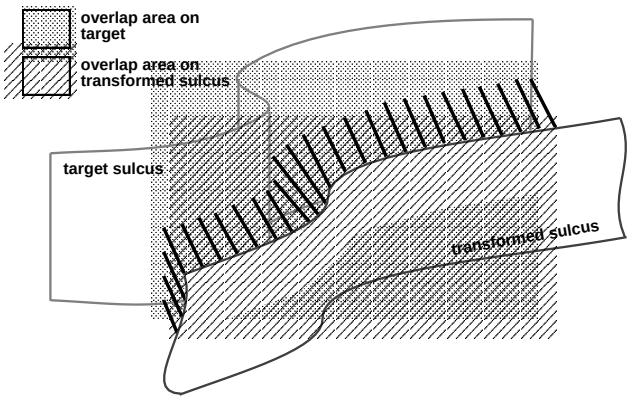

Fig. 6. The D_{surf} error measure is evaluated over the overlapping sections of two matching sulci.

IV. Experiments and Results

Two series of three experiments were completed varying only the features used by ANIMAL , i.e., intensity, gradient or labelled sulci. The first series was completed for simulated data, and the second series, for real MRI data. In each experiment, 10 MRI volumes were registered to the chosen target volume. The goal of the first experiment (Expt. I) was to demonstrate that the additional use of unlabelled sulci as features improves cortical registration over the standard technique (i.e., using blurred intensity and gradient magnitude features). In the second experiment (Expt. II), the problem of establishing correspondence is addressed by using five pairs of automatically *labelled* sulci (superior and middle frontal, Sylvian, olfactory and central, on both hemispheres) as features. The third method (Expt. III) adds all sulci automatically extracted by SEAL into the registration process after completing the ANIMAL +selected sulci (Expt. II) registration. A linear registration, using 9 degrees of freedom (3 translations, 3 rotations and 3 scales) is also presented for comparisons. Figures 7 and 8 summarize the results qualitatively for simulated and real data, respectively. Tables 1 and 2 present quantitative results for the measure described above.

A. Simulations

The images in Fig 7 demonstrate that the standard ANIMAL non-linear registration (Fig 7-b) properly accounts for global brain shape and that the main lobes are aligned since the central (purple) and Sylvian (red) sulci are better aligned than in linear registration (Fig 7-a). Quantitatively, the 38% reduction in D_{surf} (from 3.4 to 2.1mm) is highly significant ($T = 243$, $p < 0.001$;

TABLE I

RESULTS FOR SIMULATED DATA.

	lin	∇	∇+all	$\nabla + 5$	$\nabla 5a$
Central	3.2;1.5	1.2;1.4	1.0;1.2	0.7;0.3	0.7;0.4
PostCen	4.2;2.3	2.2;2.4	1.8;2.3	1.3;1.5	1.3;1.5
MidFrontal	3.2;1.0	1.4;1.2	0.8;0.9	0.7;0.6	0.7;0.6
SupFrontal	3.4;1.9	1.8;2.1	1.7;2.2	1.6;2.1	1.7;2.1
Sylvian	4.0;1.3	3.0;1.2	2.8;1.2	2.4;0.9	2.4;1.0
Olfactory	3.2;4.2	1.7;2.8	1.6;2.8	1.5;2.9	1.6;2.8
avg (n=16)	3.4;2.3	2.1;2.1	1.6;2.0	1.6;1.7	1.5;1.7

Mean and standard deviation of D_{surf} minimum distance results (mean(D_{surf});std(D_{surf})) for linear (lin), non-linear ANIMAL (∇), Expt. I: ANIMAL with all unlabelled sulci (∇+all), Expt. II: ANIMAL+selected labelled sulci (∇+5), Expt. III: ANIMAL with labelled sulci followed by all unlabelled sulci ($\nabla 5a$) registration methods. Average is computed for both left and right hemispheres for 16 sulci on 10 subjects. Only 6 of the 16 sulci are listed in the table. All measures in millimeters.

paired T-test). Even though previous experiments in [5] have shown that basal ganglia structures (e.g., thalamus, caudate, putamen, globus pallidus) and ventricular structures are well registered (with voxel overlaps on the order of 85% to 90%) for both simulated and real data, the simulations presented here indicate that the standard ANIMAL technique has difficulty registering cortical structures when using only image intensities and gradient magnitude features.

A.1 Expt. I: ANIMAL+all unlabelled sulci:

In the first experiment, adding sulci to the non-linear registration yields a significant improvement ($T = 201$, $p < 0.001$) over the standard non-linear registration by further reducing the average D_{surf} by 0.46mm, from 2.1mm to 1.6mm. Figure 7-c shows a tighter grouping of sulci, however sections of some sulci are mis-registered onto non-homologous sulci (e.g., the post-central (blue) sulci is incorrectly registered on to the central sulci (purple) for one subject; Sylvian (red)

TABLE II

RESULTS FOR REAL DATA.

	lin	∇	∇+all	$\nabla + 5$	$\nabla 5a$
Central	4.7;1.3	4.1;1.4	3.8;1.4	2.5;1.2	2.5;1.2
PostCen	6.4;1.7	6.1;2.0	6.2;2.2	5.0;1.7	5.0;1.8
MidFrontal	6.2;3.5	5.4;3.2	5.3;3.2	4.5;3.1	4.7;3.2
SupFrontal	6.2;3.8	5.6;3.6	5.3;3.8	4.4;3.9	4.4;4.0
Sylvian	5.2;1.6	5.0;1.4	4.7;1.4	3.6;0.9	3.7;1.0
Olfactory	2.1;1.7	1.6;1.9	1.4;1.9	1.3;1.6	1.4;1.8
avg (n=16)	5.0;3.2	4.5;3.1	4.3;3.2	4.0;3.1	4.0;3.1

See caption for Table I.

from one subject is not at all registered with the target).

A.2 Expt. II: ANIMAL+selected labelled sulci:

In Fig. 7-d, five pairs of sulci were labelled (superior and middle frontal, Sylvian, olfactory and central, on both hemispheres) and used as additional features in ANIMAL . This was done to address problems in establishing correspondence apparent in Expt. I. Visual inspection of Fig. 7-d shows that the previous misalignments in the motor-sensory area have been corrected (e.g., postcentral and Sylvian described above), and alignment for neighbouring structures has improved greatly. Indeed, when evaluated on the post-central sulcus, the D_{surf} measure improves dramatically: $4.2mm$ for linear; $2.2mm$ for standard non-linear; $1.8mm$ for ANIMAL with all unlabelled sulci and $1.3mm$ for ANIMAL with 5 pairs of labelled sulci. The standard deviation of D_{surf} decreases as well, indicating tighter grouping around the target sulci.

A.3 Expt. III: ANIMAL+labelled selected sulci+all unlabelled sulci:

In the last experiment, the ANIMAL +labelled selected sulci transformation was used as input to a registration strategy where all (unlabelled) sulci extracted by SEAL are used as features in an additional registration step in an attempt to further improve cortical alignment in regions that are not close to the previously selected sulci. Only a slight improvement is evident in Fig. 7-e. Table 1 shows that the average D_{surf} (taken over all sulci) is reduced from $1.6mm$ for the standard ANIMAL with selected sulci to $1.5mm$ when evaluated over all sulci and all subjects. While this reduction is small, it is statistically significant ($T = 88$, $p < 0.001$).

B. Real MRI data

When applied to real data, the image in Fig. 8-b shows that that the standard ANIMAL non-linear registration is not enough to align cortical structures between different subjects. In fact, the non-linear registration does not on inspection appear to be much better than the linear registration (Fig. 8-a) even though there is a significant ($T = 129$, $p < 0.001$) quantitative reduction of 0.49mm (from 5.0 to 4.5mm) in D_{surf} as shown in Table 2.

B.1 Expt. I: ANIMAL+all unlabelled sulci:

When all sulci are used as features in the ANIMAL registration, D_{surf} decreases by 0.71mm over linear registration (from 5.0mm to 4.3mm). Therefore, using all sulci accounts for 45% more improvement (from 4.5mm to 4.3mm) in registration over the standard non-linear procedure ($T = 109$, $p < 0.001$).

B.2 Expt. II: ANIMAL+selected labelled sulci:

Both automatic and manual labelling methods (section III-B.2.b) were used to identify the selected sulci that would take part in the registration process. Since the automatic labelling was not identical to the manual labelling, the registration results were slightly different and both are reported here.

B.2.a Automatically labelled sulci. The use of 5 pairs of automatically labelled sulci improves cortical registration significantly in the neighbourhood of the sulci chosen and this is confirmed quantitatively. When using sulci automatically identified by SEAL , D_{surf} is reduced by $0.81mm$ from $5.0mm$ with linear registration to $4.2mm$ with non-linear registration with the 5 pairs of automatically labelled sulci.

B.2.b Manually labelled sulci. Since it is possible that the automatic sulcal labelling is incorrect, and the goal of these experiments is to demonstrate improved registration using sulcal features, this experiment was repeated with manually labelled sulci. As shown in Fig. 8-d, the central sulcus (purple), superior frontal (orange), middle frontal (red), olfactory (black) and Sylvian (red) are well defined. These results are verified quantitatively in the $\nabla + 5$ column of Table 2. When using the manually labelled sulci, D_{surf} is reduced by 0.99mm — to $4.0mm$. This is more than twice the improvement of using all sulci in the registration process. It is important to note that in both cases (manual and automatic labelling), the improvement is not only local

to the selected sulci; alignment of neighbouring sulci is improved as well (e.g., postcentral sulcus in Fig. 8-d).

B.3 Expt. III: ANIMAL+selected labelled sulci+all unlabelled sulci:

When the previous result is used as input for a registration using all sulci as features, some of the other sulci come into better alignment, while others may be attracted to non-homologous sulci, since no explicit labelling of sulci is used in this step. In fact, the average registration error does not change, and remains stable at 4.0mm.

V. Discussion and Conclusion

It is well known that there exists a great deal of anatomical variability for cortical structures. There are at least two components that contribute to the measure of variablity. First, there exists variability in the position and shape of homologous gyri and sulci after spatially normalizing subjects into a standardized brain-based coordinate system. Even for primary sulci (e.g., central, Sylvian, superior frontal) there is a significant amount of variability in spatial position. For example, Talairach showed that the anterior-posterior position of the central sulcus (the main division between motor control and sensory regions) varies by more that 1.5cm [57]. Secondary and tertiary sulci are even more variable in position (and existence).

The ANIMAL procedure was designed to account for positional variability by estimating the deformation required to achieve point correspondence among individual brains. Like all image matching procedures, ANIMAL makes the operational assumption that brains are topographically equivalent when we know this to be incorrect for cortical features. The random deformations used to simulate different anatomies (section III-A.1) model only positional variability. The simulation results indicate clearly that ANIMAL can account for spatial variability, even in cases where very large deformations (greater than 30mm) are required. Furthermore, the experimental results demonstrate that these registrations improve substantially when using the extra cortical features.

The second form of variability concerns different cortical topographies. A specific anatomical region can be represented as a single gyrus in one subject while the same structure is made up of two gyri in a second subject [58]. Similarly, different sulcal patterns exist; a given sulcus can be continuous on one hemisphere and be broken into multiple folds on the other hemisphere. The simulations do not account for different topographies of gyral and sulcal patterns. Still, the

value of these simulations is not diminished since they can be used to determine a lower-bound on the registration error — corresponding to the optimal case if a true 1-to-1 mapping existed between two subjects.

When used with a single target model, ANIMAL cannot correct for this second form of variability. For example, how does one define the mapping for the region of Heschl's gyrus between a given subject and a single target, where the gyrus can be represented by a single or a double gyrus? It simply does not have the deforming power to unfold the cortex of one subject and re-fold it arbitrarily to fit the target. It is important to note that this problem affects not only ANIMAL , but all registration algorithms that are based on the 1-to-1 homology assumption. While fluid-based registration methods [29] may be able to compute a continuous mapping between these gyri, it is not clear if there even exists is a correct solution to the correspondence problem in these cases. Notwithstanding these fundamental correspondence issues, much can be achieved by heuristic approaches.

THIS TECH DOES NOT INCUR THE INCREASED COMPUTATIONAL BURDEN OF FLUID

Christensen97a examples: equiv homology on macaque + hippocampus

In future work, further improvements to the ANIMAL registration algorithm will require a slight change in fitting strategy to account for different cortical topographies apparent in real MRI data. We envision using a number of different targets simultaneously, where each target will account for a particular type of sulcal pattern for different regions of the cortex[58]. There are a number of projects ongoing in our lab to address these questions for different regions of the cortex such as orbitofrontal cortex [59], soc neurosci frontal cortex [60], [61], cingulate cortex [62], sensory motor region [63], planum templorale and Heschl's gyrus [64], area V5/MT [65], hippocampus [66]. After an initial warp, the best target (single or double Heschl's gyrus for the example above) will be selected for each sub-region to continue the procedure.

The second set of experiments demonstrate that the use of automatically extracted and labelled sulci in conjunction with a chamfer distance function can significantly improve cortical registration for real MRI data. While experimental results with real data are not as striking as the simulations, there are a number of points to keep in mind that may explain why there is a smaller improvement in registration for real data. At least three independent factors are included in the D_{surf} distance measure: 1) identification or homology error (are truly homologous

sulci being compared?), 2) extraction variability (are sulci robustly extracted by SEAL ?), and 3) registration error.

In the case of simulations, the identification error is null since homology is defined within the simulations. Identification error is certainly non-null for real data, since some sulci on some subjects are identified with small side branches, while others are not. This is due to the fact that manual identification of some sulci can be quite difficult due to normal anatomical variability, thus leading to homology errors.

There are two main directions for future work on this project. First, we plan to apply the technique to a large number of brains for evaluation and validation in the context of the ICBM project. Second, we are looking at two ways to remove the need for manual intervention. Preliminary experiments indicate that it may be possible to use sulcal characteristics (e.g., length, depth, orientation) in addition the sulcal priors used by SEAL to identify sulci and to automatically establish correspondence between (at least) the primary sulci. This would improve the completely automatic non-linear registration procedure presented here.

The current version of ANIMAL now allows the use of a chamfer-distance objective function to align sulci, however nothing in the implementation is sulci-specific. Indeed, any geometric structure that can be voxelated can be incorporated into the matching procedure to further refine the fit. We are therefore currently evaluating the incorporation of explicitly extracted cortical surfaces [44], [45].

In conclusion, we have demonstrated that incorporating cortical information represented by automatically extracted and labelled sulcal ribbons can improve registration of cortical features. If one is willing to pay a small price for manual intervention, the use of labelled sulci removes ambiguity when establishing correspondence, reduces errors due to sulcal mis-alignment and thus further improves registration.

ACKNOWLEDGMENTS

This work was supported by the NIMH-funded International Consortium for Brain Mapping as part of the Human Brain Map Project. We also acknowledge post-doctoral funding from the Human Frontier Science Project Organization (DLC). Parts of this project was funded by Medical Research Council (MRC SP-30) and an ICBM grant. We also wish to acknowledge the manual labelling of sulcal traces completed by Raghu Venegopal.

References

[1] D. Collins, G. LeGoualher, R. Venugopal, Z. Caramanos, A. C. Evans, and C. Barillot, "Cortical constraints for non-linear cortical registration," in *Proceedings of the 4th International Conference on Visualization in Biomedical Computing* (K. Höene, ed.), vol. 1131 of *Lecture Notes in Computer Science*, (Hamburg), pp. 307–316, Sept 1996.

[2] P. T. Fox, M. A. Mintun, E. M. Reiman, and M. E. Raichle, "Enhanced detection of focal brain responses using intersubject averaging and change-distribution analysis of subtracted PET images," *Journal of Cerebral Blood Flow and Metabolism*, vol. 8, pp. 642–653, 1988.

[3] A. C. Evans, S. Marrett, J. Torrescorzo, S. Ku, and L. Collins, "MRI-PET correlation in three dimensions using a volume-of-interest (VOI) atlas," *Journal of Cerebral Blood Flow and Metabolism*, vol. 11, pp. A69–78, Mar 1991.

[4] J. Mazziotta, A. Toga, A. Evans, P. Fox, and J. Lancaster, "A probabilistic atlas of the human brain: theory and rationale for its development. the international consortium for brain mapping," *NeuroImage*, vol. 2, no. 2, pp. 89–101, 1995.

[5] D. L. Collins, C. J. Holmes, T. M. Peters, and A. C. Evans, "Automatic 3D model-based neuroanatomical segmentation," *Human Brain Mapping*, vol. 3, no. 3, pp. 190–208, 1995.

[6] D. L. Collins, T. M. Peters, and A. C. Evans, "An automated 3D non-linear image deformation procedure for determination of gross morphometric variability in human brain," in *Proceedings of the 3rd International Conference on Visualization in Biomedical Computing*, SPIE, 1994.

[7] G. Borgefors, "Distance transformations in arbitrary dimensions," *Computer Graphics, Vision and Image Processing*, vol. 27, pp. 321–345, 1984.

[8] G. Borgefors, "On digital distance transforms in three dimensions," *Computer Vision Image Understanding*, vol. 64, pp. 368–76, 1996.

[9] A. C. Evans, W. Dai, D. L. Collins, P. Neelin, and T. Marrett, "Warping of a computerized 3-D atlas to match brain image volumes for quantitative neuroanatomical and functional analysis," in *Proceedings of the International Society of Optical Engineering: Medical Imaging V*, vol. 1445, (San Jose, California), SPIE, 27 February – 1 March 1991.

[10] F. Bookstein, "Thin-plate splines and the atlas problem for biomedical images," in *12th International Conference, Information Processing in Medical Imaging* (A. Colchester and D. Hawkes, eds.), vol. 511 of *Lecture Notes in Computer Science*, (Wye, UK), pp. 326–342, IPMI, Springer-Verlag, July 1991.

[11] Y. Ge, J. Fitzpatrick, R. Kessler, and R. Margolin, "Intersubject brain image registration using both cortical and subcortical landmarks," in *Proceedings of SPIE Medical Imaging*, vol. 2434, pp. 81–95, SPIE, 1995.

[12] S. Luo and A. Evans, "Matching sulci in 3D space using force-based deformation," tech. rep., McConnell Brain Imaging Centre, Montreal Neurological Institute, McGill University, Montreal, Nov 1994.

[13] S. Sandor and R. Leahy, "Towards automated labelling of the cerebral cortex using a deformable atlas," in *14th International Conference, Information Processing in Medical Imaging* (Y. Bizais, C. Barillot, and R. DiPaola, eds.), (Brest, France), pp. 127–138, IPMI, Kluwer, Aug 1995.

[14] D. Dean, P. Buckley, F. Bookstein, J. Kamath, and D. Kwon, "Three dimensional MR-based morphometric

comparison of schizophrenic and normal cerebral ventricles," in *Proceedings of the 4th International Conference on Visualization in Biomedical Computing*, vol. 1131 of *Lecture Notes in Computer Science*, pp. 363–371, Springer-Verlag, Sept. 1996.

[15] G. Christensen, S. Joshi, and M. Miller, "Volumetric transformation of brain anatomy," *IEEE Transactions on Medical Imaging*, vol. 16, no. 6, pp. 864–77, 1996.

[16] S. Joshi, M. Miller, G. Christensen, A. Banerjee, T. Coogan, and U. Grenander, "Hierarchical brain mapping via a generalized dirichlet solution for mapping brain manifolds," in *Proceedings of the SPIE's 1995 International Symposium on Optical Science, Engineering, and Instrumentation*, vol. 2573 of *Vision Geometry IV*, pp. 278–289, SPIE, Aug 1995.

[17] R. Bajcsy and S. Kovacic, "Multiresolution elastic matching," *Computer Vision, Graphics, and Image Processing*, vol. 46, pp. 1–21, 1989.

[18] G. Christensen, R. Rabbitt, and M. Miller, "3D brain mapping using a deformable neuroanatomy," *Physics in Med and Biol*, vol. 39, pp. 609–618, 1994.

[19] J. Gee, L. LeBriquer, and C. Barillot, "Probabilistic matching of brain images," in *14th International Conference, Information Processing in Medical Imaging* (Y. Bizais and C. Barillot, eds.), (Ile Berder, France), IPMI, Kluwer, July 1995.

[20] J. Zhengping and P. H. Mowforth, "Mapping between MR brain images and a voxel model," *Med Inf (Lond)*, vol. 16, pp. 183–93, Apr-Jun 1991.

[21] K. Friston, C. Frith, P. Liddle, and R. Frackowiak, "Plastic transformation of PET images," *Journal of Computer Assisted Tomography*, vol. 15, no. 1, pp. 634–639, 1991.

[22] P. Thompson and A. Toga, "A surface-based technique for warping 3-dimensional images of the brain," *IEEE Transactions on Medical Imaging*, vol. 15, no. 4, pp. 383–392, 1996.

[23] C. Davatzikos, "Spatial normalization of 3D brain images using deformable models," *J Comput Assist Tomogr*, vol. 20, pp. 656–65, Jul-Aug 1996.

[24] C. Broit, *Optimal registration of deformed images.* PhD thesis, University of Pennsylvania, Philadelphia, 1981.

[25] R. Bajcsy and C. Broit, "Matching of deformed images," in *Proceedings of the 6th International Conference on Pattern Recognition*, (Munich, Germany), pp. 351–353, IEEE, Oct 19-22 1982.

[26] R. Dann, J. Hoford, S. Kovacic, M. Reivich, and R. Bajcsy, "Three-dimensional computerized brain atlas for elastic matching: Creation and initial evaluation," in *Medical Imaging II*, vol. 0914, (Newport Beach, Calif.), pp. 600–608, SPIE, Feb. 1988.

[27] J. Gee, "Probabilistic matching of deformed images," Tech. Rep. Technical report MS-CIS-96, Department of Computer and Information Science, University of Pennsylvania, Philadelphia, 1996.

[28] M. Miller, Y. A. G.E. Christensen, and U. Grenander, "Mathematical textbook of deformable neuroanatomies," *Proceedings of the National Academy of Sciences*, vol. 90, no. 24, pp. 11944–11948, 1993.

[29] G. Christensen, R. Rabbitt, and M. Miller, "Deformable templates using large deformation kinematics," *IEEE Transactions on Image Processing*, vol. 5, no. 10, pp. 1435–1447, 1996.

[30] K. Friston, , J. Ashburner, C. Frith, J.-B. Poline, J. Heather, and R. Frackowiak, "Spatial registration and normalization of images," *Human Brain Mapping*, vol. 1, no. 2, pp. 1–25, 1995.

[31] J. Ashburner and K. Friston., "Fully three-dimensional nonlinear spatial normalisation: A new approach," in *2nd International Conference on Functional Mapping of the Human Brain* (J. Belliveau, D. Kennedy, and B. Rosen, eds.), (Boston), p. 169, Organization for Human Brain Mapping, June 1996.

[32] A. Pentland and S. Sclaroff, "Closed-form solutions for physically based shape modelling and recognition," *IEEE Transactions on Pattern Analysis and Machine Intelligence*, vol. 13, no. 7, pp. 715–729, 1991.

[33] T. Cootes, C. Taylor, and D. Cooper, "Active shape models–their training and application," *Computer Vision & Image Understanding*, vol. 61, pp. 38–59, 1995.

[34] G. Szkely, A. Kelemen, C. Brechbhler, and G. Gerig, "Segmentation of 3-D and 3-D objects from MRI volume data using constrained elastic deformations of flexible fourier contour and surface models," *Medical Image Analysis*, vol. 1, no. 1, pp. 19–34, 1996.

[35] Y. Ge, J. Fitzpatrick, B. Dawant, J. Bao, R. Kessler, and R. Margolin, "Accurate localization of cortical convolutions in mr brain images," *IEEE Transactions on Medical Imaging*, vol. 15, no. 4, pp. 418–428, 1997.

[36] G. Subsol, J.-P. Thirion, and N. Ayache, "Application of an automatically built 3D morphometric brain atlas: study of cerebral ventricle shape," in *Proceedings of the 4th International Conference on Visualization in Biomedical Computing*, vol. 1131 of *Lecture Notes in Computer Science*, pp. 373–382, Springer-Verlag, Sept. 1996.

[37] G. Subsol, N. Roberts, M. Doran, J. P. Thirion, and G. H. Whitehouse, "Automatic analysis of cerebral atrophy," *Magn Reson Imaging*, vol. 15, no. 8, pp. 917–27, 1997.

[38] R. Kwan, A. C. Evans, and G. B. Pike, "An extensible MRI simulator for post-processing evaluation," in *Proceedings of the 4th International Conference on Visualization in Biomedical Computing*, vol. 1131 of *Lecture Notes in Computer Science*, (Hamburg), pp. 135–140, September 1996.

[39] D. L. Collins, A. P. Zijdenbos, V. Kollokian, J. G. Sled, N. J. Kabani, C. J. Holmes, and A. C. Evans, "Design and construction of a realistic digital brain phantom," *IEEE Transactions on Medical Imaging*, vol. 17, no. 3, pp. 463–468, 1997.

[40] C. Sorlié, D. L. Collins, K. J. Worsley, and A. C. Evans, "An anatomical variability study based on landmarks," tech. rep., McConnell Brain Imaging Centre, Montreal Neurological Institute, McGill University, Montreal, Sept 1994.

[41] F. L. Bookstein, "Principal warps: Thin-plate splines and the decomposition of deformations," *IEEE Transactions on Pattern Analysis and Machine Intelligence*, vol. PAMI-11, no. 6, pp. 567–585, 1989.

[42] J. G. Sled, A. P. Zijdenbos, and A. C. Evans, "A non-parametric method for automatic correction of intensity non-uniformity in MRI data," *IEEE Transactions on Medical Imaging*, vol. 17, Feb. 1998.

[43] D. L. Collins, P. Neelin, T. M. Peters, and A. C. Evans, "Automatic 3D inter-subject registration of MR volumetric data in standardized talairach space," *Journal of Computer Assisted Tomography*, vol. 18, pp. 192–205, March/April 1994.

[44] D. MacDonald, D. Avis, and A. C. Evans, "Multiple surface identification and matching in magnetic resonance images," in *Proceedings of the 3rd International Conference on Visualization in Biomedical Computing*, SPIE,

1994.

[45] D. MacDonald, *Identifying geometrically simple surfaces from three dimensional data.* PhD thesis, McGill University, Montreal, Canada, December 1994.

[46] A. P. Zijdenbos, A. C. Evans, F. Riahi, J. Sled, J. Chui, and V. Kollokian, "Automatic quantification of multiple sclerosis lesion volume using stereotaxic space," in *Proceedings of the 4th International Conference on Visualization in Biomedical Computing*, vol. 1131 of *Lecture Notes in Computer Science*, pp. 439–448, Springer-Verlag, Sept. 1996.

[47] G. L. Goualher, C. Barillot, and Y. Bizais, "Three-dimensional segmentation and representation of cortical sulci using active ribbons," in *International Journal of Pattern Recognition and Artificial Intelligence*, vol. 11, pp. 1295–1315, 1997.

[48] A. C. Evans, S. Marrett, P. Neelin, D. L. Collins, K. Worsley, W. Dai, S. Milot, E. Meyer, and D. Bub, "Anatomical mapping of functional activation in stereotactic coordinate space," *NeuroImage*, vol. 1, no. 1, pp. 43–53, 1992.

[49] D. L. Collins and A. C. Evans, "Animal: validation and applications of non-linear registration-based segmentation," *International Journal and Pattern Recognition and Artificial Intelligence*, vol. 11, pp. 1271–1294, Dec 1997.

[50] G. Le Goualher, C. Barillot, Y. Bizais, and J.-M. Scarabin, "Three-dimensional segmentation of cortical sulci using active models," in *SPIE Medical Imaging*, vol. 2710, (Newport-Beach, Calif.), pp. 254–263, SPIE, 1996.

[51] F. Leitner, I. Marque, S. Lavalee, and P. Cinquin, "Dynamic segmentation: finding the edge with snake splines," in *Int. Conf. on Curves and Surfaces*, pp. 279–284, Academic Press, June 1991.

[52] G. LeGoualher, , E. Procyk, D. L. Collins, R. Venugopal, C. Barillot, and A. C. Evans, "Automated extraction and variability analysis of sulcal anatomy," *IEEE Transactions on Medical Imaging*, vol. 18, pp. 206–217, March 1999.

[53] G. Le Goualher, E. Procyk, D. L. Collins, M. Petrides, and A. C. Evans, "Sulcus extraction and automatic labelling (SEAL): I. method for mapping of sulcal neuroanatomy," in *Forth International Conference on Functional Mapping of the Human Brain* (A. C. Evans, ed.), NeuroImage, Organization for Human Brain Mapping, June 1998. abstract no. 0729.

[54] G. LeGoualher, D. L. Collins, C. Barillot, and A. C. Evans, "Automatic identification of cortical sulci using a 3d probabilistic atlas," in *Medical Image Computing and Computer-Assisted Intervention - MICCAI*, vol. 1496 of *Lecture Notes in Computer Science*, (Cambridge, MA, USA), pp. 509–518, October 1998.

[55] Z. Caramanos, R. Venugopal, D. Collins, D. MacDonald, A. Evans, and M. Petrides, "Human brain sulcal anatomy: An mri-based study," in *Third International Conference on Functional Mapping of the Human Brain*, vol. 5(4), (Copenhagen), p. S350, Human Brain Map, May 1997.

[56] D. MacDonald, "Display: a user's manual," tech. rep., McConnell Brain Imaging Centre, Montreal Neurological Institute, McGill University, Montreal, Sept 1996.

[57] J. Talairach and P. Tournoux, *Co-planar stereotactic atlas of the human brain: 3-Dimensional proportional system: an approach to cerebral imaging.* Stuttgart, New York: Georg Thieme Verlag, 1988.

[58] M. Ono, S. Kubik, and C. Abernathey, *Atlas of Cerebral Sulci.* Stuttgart: Georg Thieme Verlag, 1990.

[59] M. Chiavaras, G. Le Goualher, A. C. Evans, and M. Petrides, "The human orbitofrontal cortex: sulcal patterns and probabilistic analysis," in *Human Brain Mapping, HBM'98*, vol. 7, p. S731, 1998.

[60] W. Baaré, D. Collins, N. Kabani, D. MacDonald, C. Liu, M. Petrides, R. Kwan, and A. Evans, "Automated and manual identification of frontal lobe gyri," in *Third International Conference on Functional Mapping of the Human Brain*, vol. 5, (Copenhagen), p. S348, Human Brain Map, May 1997.

[61] E. Procyk, M. Petrides, G. L. Goualher, L. Collins, and A. Evans, "Sulcus Extraction and Automatic Labelling (SEAL) :II. Generation of Frontal Sulc i Probabilistic 3D Maps," in *Human Brain Mapping, HBM'98*, vol. 7, p. S730, 1998.

[62] T. Paus, F. Tomaiuolo, N. Otaky, D. MacDonald, M. Petrides, J. Atlas, R. Morris, and A. C. Evans, "Human cingulate and paracingulate sulci: Pattern, variability, asymmetry and probabilistic map," *Cerebral Cortex*, vol. 6, no. 2, pp. 207–14, 1996.

[63] G. L. Goualher, A. Argenti, and A. Evans, "Study of the Genetic Encoding of the Central Sulcus Shape Using Principal Component Analysis," in *Human Brain Mapping, HBM'99*, vol. 9, p. S74, 1999.

[64] V. B. Penhune, R. J. Zatorre, J. D. MacDonald, and A. C. Evans, "Interhemispheric anatomical differences in human primary auditory cortex: probabilistic mapping and volume measurement from magnetic resonance scans.," *Cerebral Cortex*, vol. 6, no. 5, pp. 661–72, 1996.

[65] S. Dumoulin, R. Bittar, N. Kabani, C. J. Baker, G. Le Goualher, G. Pike, and A. Evans, "Quantification of the variability of human area V5/MT in relation in to the sulcal pattern in the parieto-temporo-occipital cortex: a new anatomical landmark," *Cerebral Cortex*, p. accepted for publication, 1999.

[66] J. C. Pruessner, L. M. Li, W. Serles, M. Pruessner, D. L. Collins, N. J. Kabani, and A. C. Evans, "Segmentation of hippocampus and amygdala with high resolution MRI," *Cerebral Cortex*, 1999. accepted for publication.

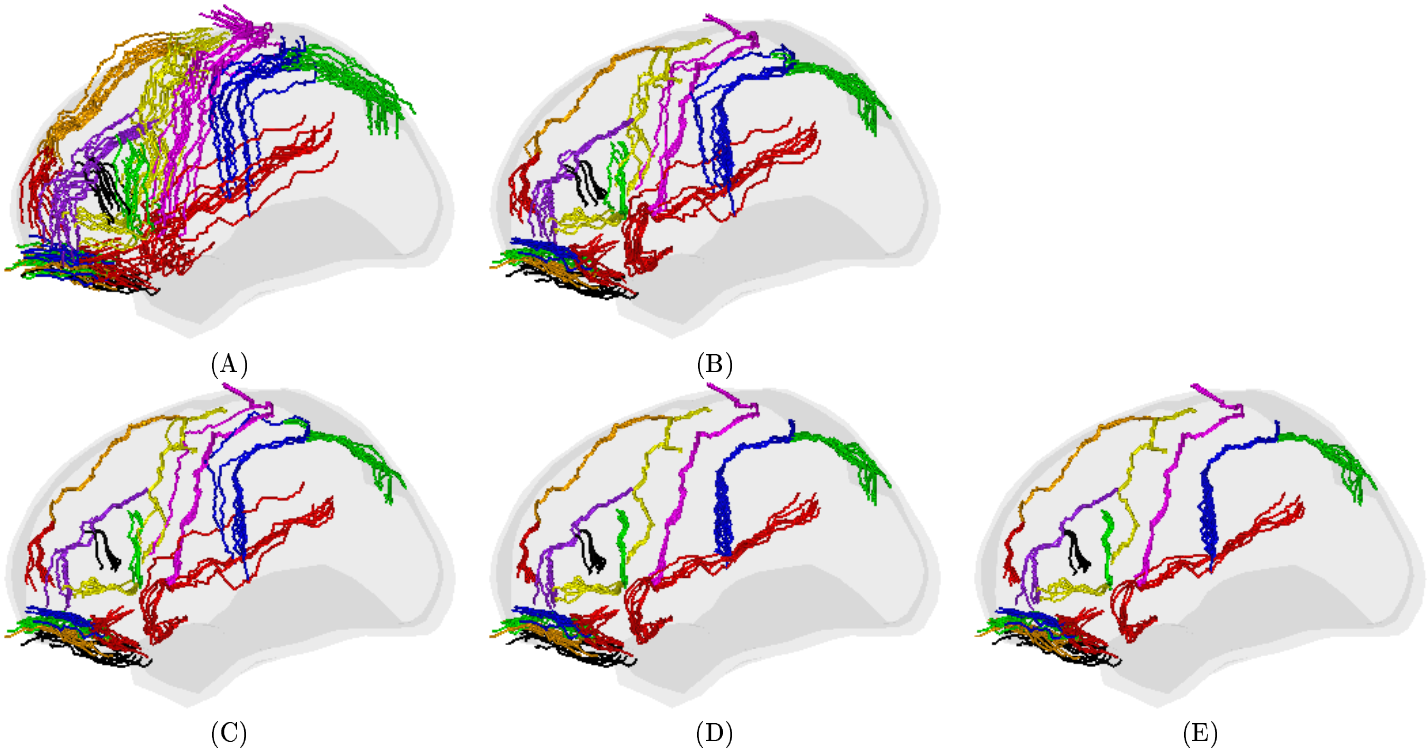

Fig. 7. Results for Simulated data: Left-side view of the cortical traces of 16 sulci from 10 simulated volumes overlaid on an average cortical surface after mapping into stereotaxic space with the different transformations described in the experiments (A-linear, B-standard non-linear, C-all unlabelled sulci, D-5 pairs of labelled sulci, E-5 pairs of labelled sulci, followed by all unlabelled sulci). These simulations show that extracted and labelled sulci improve the standard ANIMAL registrations. (Sulcal colour code is the same as for Fig 5.)

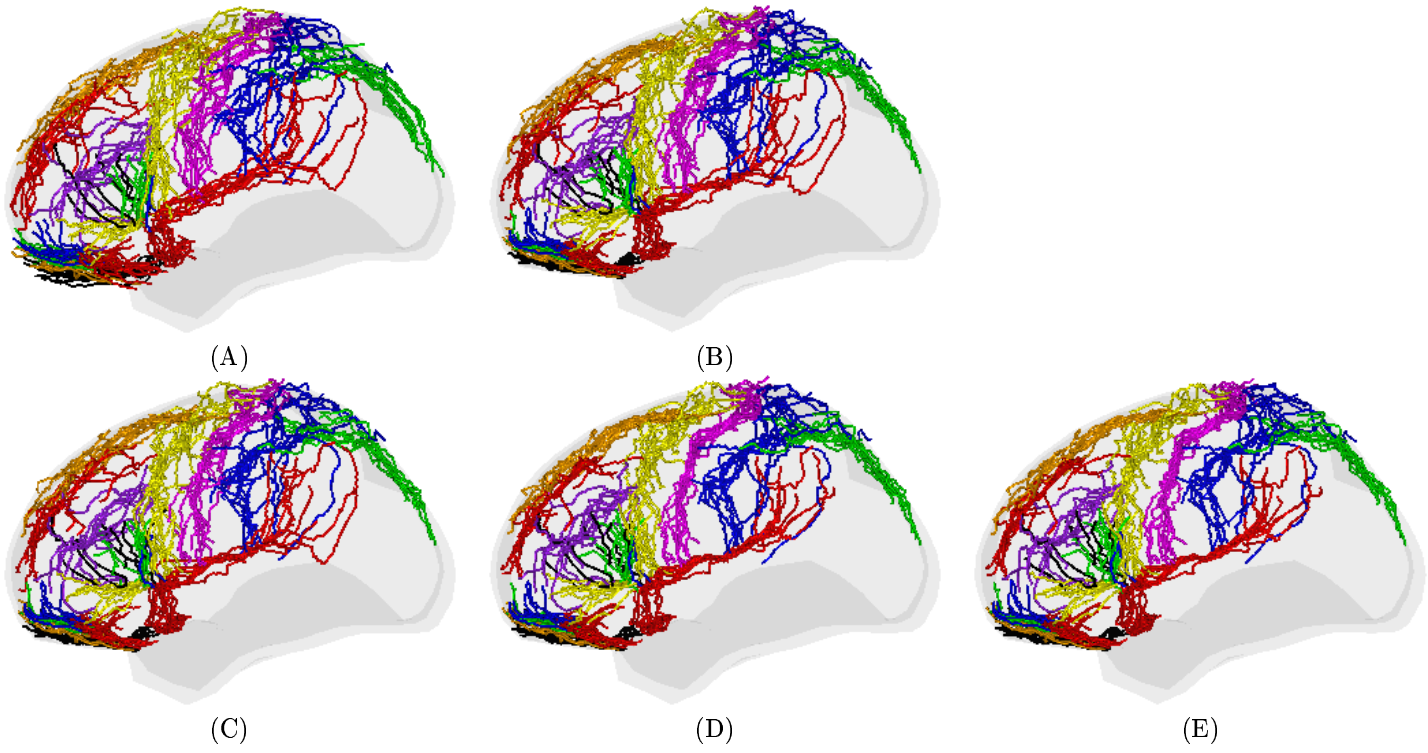

Fig. 8. Results for real data: Left-side view of the cortical traces of 16 sulci from 10 real subjects overlaid on an average cortical surface after mapping into stereotaxic space. A-E as in Fig. 7. The standard ANIMAL registration technique (B) does not deal well with cortical structures as there is little improvement over linear registration (A). The addition of sulcal constraints (C-E) improves cortical registration over the standard ANIMAL non-linear technique (B). Registrations using 5 pairs of labelled sulci (D,E) yield significantly better cortical alignment since sulcal correspondence is accounted for. (Sulcal colour code is the same as for Fig 5.)